Dyes and Pigments 243 (2025) 113053

Contents lists available at ScienceDirect

Dyes and Pigments

journal homepage: www.elsevier.com/locate/dyepig

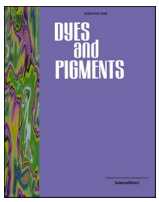

Unlocking room temperature phosphorescence in dibenzothiophene-based systems via the Scholl reaction

Clara Fabregat [a,b,1], Roger Bujaldón [a,b,1], Jaume Garcia-Amorós [a,b], Dmytro Volyniuk [c], Melika Ghasemi [c], Juozas V. Grazulevicius [c], Dolores Velasco [a,b,*]

[a] Grup de Materials Orgànics, Departament de Química Inorgànica i Orgànica, Secció de Química Orgànica, Universitat de Barcelona, Martí i Franquès 1, E-08028, Barcelona, Spain
[b] Institut de Nanociència i Nanotecnologia (IN^{2}UB), E-08028, Barcelona, Spain
[c] Department of Polymer Chemistry and Technology, Kaunas University of Technology, Radvilenu Plentas 19, LT-50254, Kaunas, Lithuania

ARTICLE INFO

Keywords:
diphenanthro[9,10-*b*:9′,10′-*d*]thiophene
Organic optoelectronics
p-type semiconductors
Room temperature phosphorescence
White light

ABSTRACT

A family of butterfly-shaped diphenanthro[9,10-*b*:9′,10′-*d*]thiophene derivatives has been straightforwardly synthesized from tetrabromothiophene via consecutive Suzuki-Miyaura and Scholl reactions, targeting potential charge-transporting and light-emitting organic materials. Indeed, time of flight measurements displayed hole mobility values up to 4.7×10^{-5} cm^2 V^{-1} s^{-1} under an applied electric field of 6×10^5 V cm^{-1}. Spectroscopic studies showed promising photoluminescence, with quantum yields up to 27.5 % and adjustable emissions ranging from deep blue to sky blue in solution and in solid films, respectively. Moreover, the synthesized compounds revealed room-temperature phosphorescence when introduced as dopants in Zeonex films, a highly sought-after characteristic in metal- and halogen-free organic materials. This phenomenon delineates a spectral transition from deep blue to warm-white emission as the environment shifts from air-equilibrated to vacuum conditions, which entails different applications such as lighting or oxygen-sensing devices. Phosphorescence, which was further corroborated in dilute solutions of THF at 77 K, does not occur on the non-cyclized synthetic precursors, demonstrating the key role of the Scholl reaction to unlock it. These findings make evidence of the potential of this core for advancing optoelectronic device functionalities.

1. Introduction

Organic semiconductors (OSCs) are extensively sought materials for emerging optoelectronics. The discovery of conductivity in organic compounds derived from anthracene a century ago triggered research into new high-performance OSCs, which has since then increased exponentially in today's society [1–3]. Even if OSCs are outshone by inorganic-based semiconductors in terms of electrical performance and stability [4,5], they give access to the design of flexible and lightweight displays with reduced dimensions [6,7]. Therefore, the search for OSCs with higher charge mobilities is crucial for their implementation in next generation technologies. Besides, the electronic and optical properties of these materials can be readily fine-tuned through chemical modifications, leading to a vast array of tailored structures featuring the desired properties. OSCs find applications in diverse electronic devices including organic light-emitting diodes (OLEDs) [8,9], organic field-effect transistors (OFETs) [10–12], and organic photovoltaic cells (OPVs) [13,14]. In the former, efficient and precise photoluminescence (PL) is required. A special case resides on organic luminophores that possess room temperature phosphorescence (RTP), which are highly demanded for certain applications such as oxygen sensing, bio-imaging, molecular logic computation and data encryption, due to their high sensitivity towards temperature and oxygen [15–19]. This radiative decay occurs from the first excited triplet (T_1) to the ground state (S_0) of the molecule. Materials exhibiting RTP are distinguished by their unique emission spectra, extended emission lifetimes, and pronounced environmental sensitivity. The design of RTP emitters devoid of metals and halogens is pivotal for the fabrication of cost-effective, biocompatible and environmentally-friendly materials [20–24]. However, achieving RTP in such systems presents a considerable challenge due to the

* Corresponding author. Grup de Materials Orgànics, Departament de Química Inorgànica i Orgànica, Secció de Química Orgànica, Universitat de Barcelona, Martí i Franquès 1, E-08028, Barcelona, Spain
E-mail address: dvelasco@ub.edu (D. Velasco).
[1] These authors contributed equally to this work.

https://doi.org/10.1016/j.dyepig.2025.113053
Received 19 December 2024; Received in revised form 18 July 2025; Accepted 19 July 2025
Available online 22 July 2025

inherently weak spin-orbit coupling, which limits intersystem crossing. Apart from this, applications in multifunctional materials generally compel OSCs to offer reliable charge transport characteristics.

Thiophene is a versatile building block in the architecture of organic optoelectronics such as activated delayed fluorescence (TADF)-based OLEDs prototypes, due to its notable polarizability, electron-donating properties and the S–S nonbonding intermolecular interactions [25–28]. While traditionally valued for charge transport in OSCs [29,30], thiophene's potential for RTP applications has gained attention due to the presence of sulfur lone pair electrons, which enhances spin-orbit coupling and facilitate ISC, in line with El-Sayed's rule [31–33]. Specifically, dibenzo[*b*,*d*]thiophene (DBT) has demonstrated dual fluorescence and phosphorescence emission as a fully organic material. DFT calculations also support these findings, indicating that DBT features T_1 and T_2 states that support ISC between S_n and T_n states, with small $S_1 \rightarrow T_1$ energy gaps (ΔE_{ST}) of 0.99 (experimentally) and 0.80 eV (DFT calculations) [34]. In contrast, more twisted analogues like 2,5-diphenylthiophene or 2,2′-bibenzo[*b*]thiophene with higher ΔE_{ST} fail to exhibit RTP, highlighting the role of structural rigidity in promoting triple-state harvesting [35,36]. In this line, we propose the study of a more π-extended and branched aromatic π-core integrating DBT to potentially favor phosphorescence. More precisely, we synthesized a family of butterfly-shaped diphenanthro[9,10-*b*:9′,10′-*d*]thiophene derivatives featuring diverse functionalization patterns through a straightforward synthetic pathway (Fig. 1). Unlike other strategies [37,38], this methodology not only provides the targeted products in higher yields, but also allows for easier cost-effective side-group engineering by using readily available and inexpensive arylboronic acids as starting materials [39–42]. From the unsubstituted precursor **1a**, the nucleus was strategically functionalized with either aliphatic groups (**1b** and **1c**), more electron-donating groups like methoxy (**1d**) or an electron-withdrawing one like fluorine (**1e**), with phenyl (**1f**) and 4-(diphenylamino)phenyl (**1g**) to provide additional aromatic extension. These proposed modifications can shed light on the effectiveness of the Scholl reaction on this core as well as fine-tuning the charge transport and optical properties of diphenanthro[9,10-*b*:9′,10′-*d*]thiophene. Some butterfly-shaped thiophene-based compounds have been recently documented in the literature for diverse applications [40–43], yet with limited insight into RTP, highlighting the significance of further investigation on this topic.

This paper details the synthesis of a series of homogeneously substituted diphenanthro[9,10-*b*:9′,10′-*d*]thiophene derivatives (**2**) for potential utility in light-emitting applications and charge transporting materials. The study surveys the impact of core functionalization, assessed through electrochemical, charge mobility and photophysical characterization. The optical properties of the prepared derivatives were examined in aerated and oxygen-depleted conditions of diluted solutions, drop-casted films and Zeonex films. Additionally, the effect of the temperature in the measurements was also investigated to further elucidate the photophysical behavior of this family of compounds. The study also extended to the non-cyclized intermediates (**1**) to assess the influence of the molecular rigidity of the diphenanthro[9,10-*b*:9′,10′-*d*] thiophene scaffold on their PL behavior.

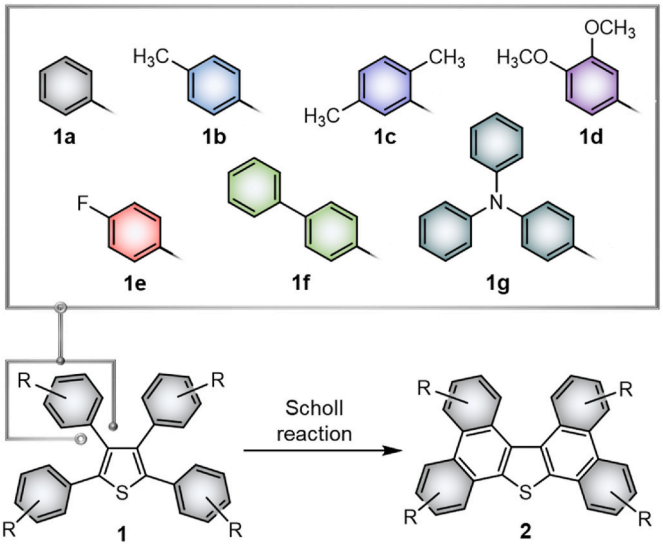

Fig. 1. General cyclization of the tetraphenylthiophene intermediate (**1**) to the diphenanthro[9,10-*b*:9′,10′-*d*]thiophene core (**2**) via the Scholl reaction. The proposed aryl moieties attached to the thiophene heterocycle to form intermediates **1a**–**g** are also specified.

2. Experimental section

2.1. Instrumentation and methods

All reagents were of commercial grade and used without further purification. Anhydrous dichloromethane was distilled over CaH_2 prior to use. Reaction progress was monitored by thin layer chromatography (TLC) on aluminum sheets pre-coated with silica gel (Merck, 60 F_{254}), with visualization achieved under ultraviolet light (254 nm). Flash column chromatography was conducted using commercially available silica gel (VWR, 40–63 μm).

^{1}H NMR spectra were acquired either in a Varian Mercury or a Bruker Advance III instrument (400 MHz). ^{13}C NMR spectra were acquired using a Bruker Advance III spectrometer operating at 100 MHz. The NMR spectra were processed with the MestReNova software (version 14.0.0–23239) and referenced using the solvent signal.

Mass spectrometry derived from matrix-assisted laser desorption/ionization time of flight (MALDI-TOF) was performed on an Applied Biosystems MDS SCIEX 4800 equipment in the reflector mode. High resolution mass spectrometry (HRMS) was performed on a LC/MSD-TOF Agilent Technologies instrument by the electrospray ionization (ESI) technique.

Thermogravimetric analysis was performed using a TA Instruments Q50 instrument at a heating rate of 10 °C min^{-1} under nitrogen atmosphere.

Cyclic voltammograms were obtained using a microcomputer-controlled potentiostat/galvanostat Autolab with PGSTAT30 equipment and GPES software (version 4.9) in a cylindrical three-electrode cell. The reference was an Ag/Ag$^+$ electrode (10^{-3} M $AgNO_3$ in acetonitrile), the working electrode was a glassy-carbon electrode, and the counter electrode was a platinum wire. The compounds were dissolved in distilled dichloromethane (10^{-3} M) and tetrabutylammonium hexafluorophosphate (TBAP, 0.1 M) was employed as the supporting electrolyte. All voltammograms were collected under quiescent conditions and under argon atmosphere at a scan rate of 100 mV s^{-1}. The resulting potentials were referred to the Fc$^+$/Fc redox couple. The ionization potentials (IP_{CV}) were estimated from the onset of the first oxidation peak (E^{ox}_{onset}) as $IP_{CV} = E^{ox}_{onset} + 5.39$, where 5.39 eV corresponds to the formal potential in the Fermi scale of the Fc$^+$/Fc couple [44]. The electron affinities (EA) were estimated as $EA = IP_{CV} - E^{opt}_{gap}$. The optical gap energies (E^{opt}_{gap}) were estimated from the λ_{onset} of the absorption spectra.

Ionization potential of the solid samples (IP_{PE}) were obtained by photoemission spectroscopy in air using a setup composed by an ASBN-D130-CM deep UV deuterium light source, a CM110 1/8 m monochromator and a 6517B Keithley electrometer. The samples were vacuum-deposited onto fluorine-doped tin oxide coated glass slides as substrates. The photoelectron emission spectra were recorded exciting the samples from low to high energies with a step of 1 nm and recording the electron photoemission current as a function of the excitation energy.

The samples for time of flight (TOF) measurements were thermally

evaporated under vacuum on 100 nm indium-tin oxide (ITO) coated glass substrates with a base pressure under 10^{-6} mbar. Then, the aluminum electrodes (70 nm) were deposited also by vacuum evaporation using a mask. A pulsed Nd:YAG laser EKSPLA NL300 ($\lambda_{Exc} = 355$ nm, pulse duration 3–6 ns) was used to generate the charge carriers in the samples. The voltage at the sample surface was adjusted using a Keithley 6517B electrometer and the photocurrent transients were recorded with a Tektronix TDS 3032C oscilloscope. The transit time (t_t) was determined from the kink on the curve of the transient in the log–log scale. The drift mobility was calculated as $\mu = d^2/Ut_t$, where d is the layer thickness and U is the surface potential at the moment of illumination. The thickness of the layers was measured using a Profilm3D profilometer. Zero-field mobilities (μ_0) and the field dependence parameter (α) were calculated as calculated as $\mu = \mu_0\, exp(\alpha E^{1/2})$, where E is the applied electric field.

Absorption spectra in dichloromethane (10 μM) were recorded in a Varian Cary UV–Vis–NIR 500E spectrophotometer. The films of the compounds were prepared by drop casting, that is, a toluene solution containing the fluorophore (1 mg/mL) was dropped onto a quartz substrate to cover all the surface and left it slowly evaporate to promote film formation. Measurements in the solid state were performed using a PerkinElmer Lambda 35 spectrophotometer. All experiments in solution were carried out using quartz cells (Hellma) with an optical path of 1 cm.

Photoluminescence spectra were recorded using an Edinburgh Instruments FLS980 fluorescence spectrophotometer. The PL of all derivatives was studied in dichloromethane solution, films and Zeonex-doped films containing 1 wt% of the fluorophore under air equilibrated and vacuum conditions. Zeonex-doped films were also prepared by drop casting, using a toluene solution containing Zeonex (4 mg/mL) and the fluorophore (1 wt% with respect to Zeonex). Photoluminescence quantum yields (PLQY) were quantified using an integrating sphere. Photoluminescence decay curves of Zeonex-doped films were measured at room temperature using the PicoQuant LDH-D-C-375 laser (λ_{Exc} = 374 nm) as the excitation source. The PL decays were fitted to mono and double exponential decay functions for phosphorescence and fluorescence, respectively. In the former case, the average lifetime was calculated using the intensity average lifetime Equation (1):

$$< \tau >_f = \frac{\int_0^x t \sum a_i\, exp(-t/\tau_i)dt}{\int_0^x \sum a_i\, exp(-t/\tau_i)dt} = \frac{\sum a_i {\tau_i}^2}{\sum a_i \tau_i} \quad (1)$$

The correlated color temperature (CCT) was calculated from the McCamy's approximation [45] using Equations (2) and (3)

$$n = \frac{(x - x_e)}{(y_e - y)} \quad (2)$$

$$CCT = an^3 + bn^2 + cn + d \quad (3)$$

where x and y represent the given CIE coordinates, x_e and y_e correspond to the coordinates of the epicenter with values of 0.3320 and 0.1858, respectively, and constants a, b, c and d are estimated as 437, 3601, 6861 and 5517, respectively.

2.2. Synthetic procedure

General procedure for the Suzuki coupling **(1a–g)**: Tetrabromothiophene (1 equiv.), arylboronic acid (4.5 equiv.), $Pd(PPh_3)_2Cl_2$ (5 % mol), PPh_3 (10 % mol) and K_2CO_3 (20 equiv.) were dissolved in a mixture of DMF and H_2O (22.5 mL, 8:1 v/v) under nitrogen and stirred at 110 °C overnight. After cooling to room temperature, the reaction mixture was diluted with water and the resulting precipitate was filtered off and dried. The solid was purified by flash column chromatography to give the corresponding tetrasubstituted thiophene.

2.2.1. Synthesis of 2,3,4,5-tetraphenylthiophene (1a)

Tetrabromothiophene (0.402 g, 1.01 mmol) and phenylboronic acid (0.554 g, 4.54 mmol) were used. The solid was purified by flash column chromatography using hexane as eluent to obtain **1a** as a white solid in a yield of 62 % (0.241 g, 0.620 mmol). ^{1}H NMR (400 MHz, $CDCl_3$) δ (ppm): 7.25–7.18 (m, 10H), 7.15–7.08 (m, 6H), 6.99–6.94 (m, 4H).

2.2.2. Synthesis of 2,3,4,5-tetra(4-tolyl)thiophene (1b)

Tetrabromothiophene (0.400 g, 1.00 mmol) and 4-tolylboronic acid (0.633 g, 4.66 mmol) were used. The solid was purified by flash column chromatography using hexane as eluent to obtain **1b** as a white solid in a yield of 67 % (0.296 g, 0.666 mmol). ^{1}H NMR (400 MHz, $CDCl_3$) δ (ppm): 7.11 (d, J = 8.1 Hz, 4H), 7.02 (d, J = 8.1 Hz, 4H), 6.92 (d, J = 8.0 Hz, 4H), 6.84 (d, J = 8.0 Hz, 4H), 2.30 (s, 6H), 2.26 (s, 6H).

2.2.3. Synthesis of 2,3,4,5-tetra(2,5-dimethylphenyl)thiophene (1c)

Tetrabromothiophene (0.400 g, 1.00 mmol) and 2,5-dimethylphenylboronic acid (0.670 g, 4.47 mmol) were used. The solid was purified by flash column chromatography using hexane as eluent to obtain **1c** as a white solid in a yield of 69 % (0.343 g, 0.685 mmol).^{1}H NMR (400 MHz, $CDCl_3$) δ (ppm): 7.10–7.04 (m, 2H), 7.00–6.91 (m, 4H), 6.82–6.66 (m, 6H), 2.22 (s, 3H), 2.21 (s, 3H), 2.16 (s, 3H), 2.14 (s, 3H), 2.08 (s, 3H), 2.05 (s, 3H), 1.93 (s, 3H), 1.79 (s, 3H).

2.2.4. Synthesis of 2,3,4,5-tetra(3,4-dimethoxyphenyl)thiophene (1d)

Tetrabromothiophene (0.605 g, 1.51 mmol) and 3,4-dimethoxyphenylboronic acid (1.23 g, 6.76 mmol) were used. The solid was purified by flash column chromatography using a mixture of hexane and dichloromethane (10:1 v/v) as eluent to obtain **1d** as a pale brown solid in a yield of 65 % (0.613 g, 0.975 mmol). ^{1}H NMR (400 MHz, $CDCl_3$) δ (ppm): 6.92 (dd, J = 8.4, 2.0 Hz, 2H), 6.77 (d, J = 8.4 Hz, 2H), 6.73 (d, J = 2.0 Hz, 2H), 6.68 (d, J = 8.2 Hz, 2H), 6.58 (dd, J = 8.2, 1.9 Hz, 2H), 6.52 (d, J = 1.9 Hz, 2H), 3.87 (s, 6H), 3.82 (s, 6H), 3.59 (s, 6H), 3.52 (s, 6H).

2.2.5. Synthesis of 2,3,4,5-tetra(4-fluorophenyl)thiophene (1e)

Tetrabromothiophene (0.402 g, 1.01 mmol) and 4-fluorophenylboronic acid (0.711 g, 5.08 mmol) were used. The solid was purified by flash column chromatography using hexane as eluent to obtain **1e** as a white solid in a yield of 66 % (0.306 g, 0.664 mmol). ^{1}H NMR (400 MHz, $CDCl_3$) δ (ppm): 7.17 (dd, J = 8.8, 5.3 Hz, 4H), 6.94 (dd, J = 8.8, 8.5 Hz, 4H), 6.91–6.81 (m, 8H).

2.2.6. Synthesis of 2,3,4,5-tetra([1,1′-biphenyl]-4-yl)thiophene (1f)

Tetrabromothiophene (0.400 g, 1.00 mmol) and 4-biphenylboronic acid (0.930 g, 4.70 mmol) were used. The solid was purified by flash column chromatography using hexane and dichloromethane (3:1 v/v) as eluent to obtain **1f** as a pale yellow solid in a yield of 81 % (0.563 g, 0.813 mmol). ^{1}H NMR (400 MHz, $CDCl_3$) δ (ppm): 7.62–7.56 (m, 8H), 7.50 (d, J = 8.4 Hz, 4H), 7.46–7.41 (m, 8H), 7.41–7.35 (m, 8H), 7.35–7.27 (m, 4H), 7.12 (d, J = 8.4 Hz, 4H).

2.2.7. Synthesis of 2,3,4,5-tetra(4-(diphenylamino)phenyl)thiophene (1g)

Tetrabromothiophene (0.397 g, 0.993 mmol) and 4-(diphenylamino) phenyl boronic acid (1.28 g, 4.44 mmol) were used. The solid was purified by flash column chromatography using a mixture of hexane and dichloromethane (10:1 v/v) as eluent to obtain **1g** as a bright yellow solid in a yield of 73 % (0.772 g, 0.730 mmol). ^{1}H NMR (400 MHz, $CDCl_3$) δ (ppm): 7.22–7.15 (m, 6H), 7.15–7.07 (m, 12H), 7.06–7.01 (m, 8H), 6.99–6.88 (m, 18H), 6.88–6.80 (m, 12H). MS (MALDI-TOF) (m/z): calculated for $C_{76}H_{56}N_4S$: 1056.4 $(M)^{\bullet+}$; found: 1056.5.

2.2.8. Synthesis of 2,5-di([1,1′-biphenyl]-2-yl)thiophene (3)

2,5-dibromothiophene (0.363 g, 1.50 mmol), 2-biphenylboronic acid (0.717 mg, 3.62 mmol), $Pd(PPh_3)_4$ (0.087 g, 0.075 mmol) and K_2CO_3 (2.07 g, 15.0 mmol) were dissolved in a mixture of THF and H_2O (52.5 mL, 6:1 v/v) under nitrogen and stirred at 80 °C for 24 h. After cooling to room temperature, the organic layer was extracted with

dichloromethane, dried over anhydrous $MgSO_4$, filtered off and the solvent was distilled off under reduced pressure. The solid was purified by flash column chromatography using a mixture of hexane and dichloromethane (10:1 v/v) as the eluent to obtain compound **3** as a white solid in a yield of 86 % (0.500 g, 1.29 mmol). ^{1}H NMR (400 MHz, $CDCl_3$) δ (ppm): 7.49–7.44 (m, 2H), 7.37–7.33 (m, 6H), 7.31–7.27 (m, 6H), 7.25–7.21 (m, 4H), 6.37 (s, 2H).

General procedure for the Scholl reaction (**2a–f**): tetrasubstituted (**1a–f**) or disubstituted thiophene (**3**) (1 equiv.) was dissolved in anhydrous dichloromethane (15 mL) under nitrogen atmosphere. Then, a previously purged solution of anhydrous $FeCl_3$ (18 equiv.) in nitromethane (5 mL) was added and the mixture was stirred at room temperature or at 0 °C. After, the reaction was diluted with methanol and the resultant precipitate was filtered off and thoroughly washed with the same solvent. The precipitate was dried to give the corresponding compound.

2.2.9. Synthesis of diphenanthro[9,10-b:9′,10′-d]thiophene (2a)

1a (0.194 g, 0.500 mmol) and anhydrous $FeCl_3$ (1.46 g, 9.00 mmol) in anhydrous dichloromethane (15 mL) and nitromethane (5 mL) was stirred for 1.5 h. The precipitate was thoroughly washed with methanol and dried. The reaction provided a complex mixture of by-products from which the expected compound **2a** could not be isolated nor quantified. Alternatively, **3** (0.153 g, 0.394 mmol) and anhydrous $FeCl_3$ (1.18 g, 7.34 mmol) in anhydrous dichloromethane (11 mL) and nitromethane (3.4 mL) was stirred for 15 min at 0 °C. The precipitate was thoroughly washed with methanol and dried. The crude product was purified by flash column chromatography using a mixture of hexane and dichloromethane (10:1 v/v) as the eluent to obtain **2a** as a white solid in a yield of 89 % (135 mg, 0.351 mmol). ^{1}H NMR (400 MHz, $CDCl_3$) δ (ppm): 8.81–8.71 (m, 6H), 8.32–8.24 (m, 2H), 7.76–7.66 (m, 6H), 7.60–7.52 (m, 2H). ^{13}C NMR (101 MHz, $CDCl_3$) δ (ppm): 137.5, 131.9, 130.2, 129.9, 129.3, 128.3, 127.6, 127.1, 127.0, 126.2, 125.4, 124.8, 124.0, 123.6. MS (ESI) (*m*/z): calculated for $C_{28}H_{16}S$: 385.1045 $(M + H)^+$; found: 385.1059.

2.2.10. Synthesis of 3,6,12,15-tetramethyldiphenanthro[9,10-b:9′,10′-d]thiophene (2b)

1b (0.223 g, 0.502 mmol) and anhydrous $FeCl_3$ (1.46 g, 9.00 mmol) in anhydrous dichloromethane (15 mL) and nitromethane (5 mL) was stirred for 5 h at room temperature. The precipitate was thoroughly washed with methanol and dried. Compound **2b** was obtained as a pale-yellow solid in a yield of 90 % (0.199 g, 0.452 mmol). ^{1}H NMR (400 MHz, $CDCl_3$) δ (ppm): 8.65 (d, J = 8.4 Hz, 2H), 8.51 (s, 4H), 8.12 (d, J = 8.2 Hz, 2H), 7.50 (dd, J = 8.4, 1.2 Hz, 2H), 7.36 (dd, J = 8.2, 1.5 Hz, 2H), 2.66 (s, 6H), 2.65 (s, 6H). ^{13}C NMR (101 MHz, $CDCl_3$) δ (ppm): 136.5, 136.3, 135.4, 131.2, 130.1, 129.7, 128.9, 127.4, 126.9, 126.6, 126.4, 124.5, 123.6, 123.3, 22.3, 22.0. MS (ESI) (*m*/z): calculated for $C_{32}H_{24}S$: 441.1671 $(M + H)^+$; found: 441.1680.

2.2.11. Synthesis of 1,4,5,8,10,13,14,17-octamethyldiphenanthro[9,10-b:9′,10′-d]thiophene (2c)

1c (0.250 g, 0.500 mmol) and anhydrous $FeCl_3$ (1.46 g, 9.00 mmol) in anhydrous dichloromethane (15 mL) and nitromethane (5 mL) was stirred for 1.5 h. The precipitate was thoroughly washed with methanol and dried. The reaction provided a complex mixture of by-products in which the target compound **2c** was not detected. Alternatively, the structure of the minor by-product **2c'** could be identified by means of its single crystal.

2.2.12. Synthesis of 2,3,6,7,11,12,15,16-octamethoxydiphenanthro[9,10-b:9′,10′-d]thiophene (2d)

1d (0.459 g, 0.730 mmol) and anhydrous $FeCl_3$ (2.13 g, 13.1 mmol) in anhydrous dichloromethane (22 mL) and nitromethane (7.5 mL) was stirred for 7 h. The precipitate was thoroughly washed with methanol and dried. Compound **1d** was obtained as a white solid in a yield of 92 % (0.491 g, 0.671 mmol). ^{1}H NMR (400 MHz, $CDCl_3$) δ (ppm): 8.12 (s, 2H), 7.91 (s, 2H), 7.90 (s, 2H), 7.54 (s, 2H), 4.18 (s, 12H), 4.16 (s, 6H), 3.85 (s, 6H). ^{13}C NMR (101 MHz, $CDCl_3$) δ (ppm): 149.5 (2C), 148.3, 146.8, 134.5, 129.8, 124.4, 123.6, 123.1, 122.4, 108.9, 105.0, 104.3, 104.1, 56.4, 56.2 (2C), 56.0. MS (ESI) (*m*/z): calculated for $C_{36}H_{32}O_8S$: 624.1812 $(M)^{\bullet+}$; found: 624.1831.

2.2.13. Synthesis of 3,6,12,15-tetrafluorodiphenanthro[9,10-b:9′,10′-d]thiophene (2e)

1e (0.230 g, 0.500 mmol) and anhydrous $FeCl_3$ (1.46 g, 9.00 mmol) in anhydrous dichloromethane (15 mL) and nitromethane (5 mL) was stirred for 72 h. The precipitate was thoroughly washed with methanol and dried. Compound **2e** was obtained as a white solid in a yield of 33 % (76.0 mg, 0.166 mmol). ^{1}H NMR (400 MHz, $CDCl_3$) δ (ppm): 8.68 (dd, J = 9.1, 5.8 Hz, 2H), 8.27–8.19 (m, 6H), 7.52–7.46 (d, J = 2.4 Hz, 2H), 7.39–7.31 (m, 2H). The ^{13}C NMR spectrum of **2e** could not be obtained due to its low solubility in the common deuterated solvents.

2.2.14. Synthesis of 3,6,12,15-tetraphenyldiphenanthro[9,10-b:9′,10′-d]thiophene (2f)

1f (0.348 g, 0.502 mmol) and anhydrous $FeCl_3$ (1.46 g, 9.00 mmol) in anhydrous dichloromethane (15 mL) and nitromethane (5 mL) was stirred for 3.5 h. The precipitate was thoroughly washed with methanol and dried. Compound **2f** was obtained as a pale yellow solid in a yield of 77 % (0.267 g, 0.388 mmol). ^{1}H NMR (400 MHz, $CDCl_3$) δ (ppm): 8.90 (d, J = 1.7 Hz, 2H), 8.88 (d, J = 1.7 Hz, 2H), 8.78 (d, J = 8.5 Hz, 2H), 8.22 (d, J = 8.2 Hz, 2H), 7.88 (dd, J = 8.2, 1.7 Hz, 2H), 7.85−7.77 (m, 8H), 7.76 (dd, J = 8.5, 1.7 Hz, 2H), 7.58−7.52 (m, 8H), 7.49−7.42 (m, 4H). ^{13}C NMR (101 MHz, $CDCl_3$) δ (ppm): 141.2 (2C), 139.4, 138.2, 137.1, 131.3, 130.3, 129.8, 129.1 (4C), 128.3, 127.3 (2C), 126.5, 124.9, 124.3, 122.0, 121.7. MS (ESI) (*m*/z): calculated for $C_{52}H_{32}S$: 689.2297 $(M + H)^+$; found: 689.2306.

2.2.15. Synthesis of 3,6,12,15-tetra(N,N-diphenylamino)diphenanthro[9,10-b:9′,10′-d]thiophene (2g)

1g (0.173 g, 0.163 mmol) and anhydrous $FeCl_3$ (0.526 g, 3.27 mmol) in anhydrous dichloromethane (5 mL) and nitromethane (1.6 mL) was stirred for 4 h. The precipitate was thoroughly washed with methanol and dried. The reaction provided a complex mixture of by-products in which the expected compound **2g** was not detected.

3. Results and discussion

3.1. Synthesis

The synthesis of the diphenanthro[9,10-*b*:9′,10′-*d*]thiophene derivatives was achieved through a two-step approach, consisting of a fourfold Suzuki-Miyaura cross-coupling reaction followed by a twofold intramolecular oxidative cyclization via the Scholl reaction (Scheme 1). As abovementioned, the coupling was performed with phenylboronic acid for the unsubstituted structure (**1a**) as well as with alternative arylboronic acids to introduce diverse substituents in different positions. Specifically, these included methyl groups in either positions 4 (**1b**) or 2 and 5 (**1c**), methoxy groups in positions 3 and 4 (**1d**) and electron-withdrawing fluorine groups in *para* (**1e**). The study also encompassed compounds featuring a higher π-extension by coupling biphenyl (**1f**) and 4-(diphenylamino)phenyl (**1g**) units, being the latter a recognized moiety for its consistent contribution to PL and aggregation-induced emission (AIE) [46–48].

The corresponding aryl groups were attached to tetrabromothiophene (TBT) in excellent yields using reported conditions [49], ranging from 62 to 81 % for the simultaneous tetra-substitution to compounds **1a**–**g**. The cyclization step was especially favorable for derivatives **2b**, **2d** and **2f**, demonstrating the efficacy of strategically-placed directing groups. Indeed, the synthesis of **2d** only produced the indicated regioisomer in an excellent 92 % yield,

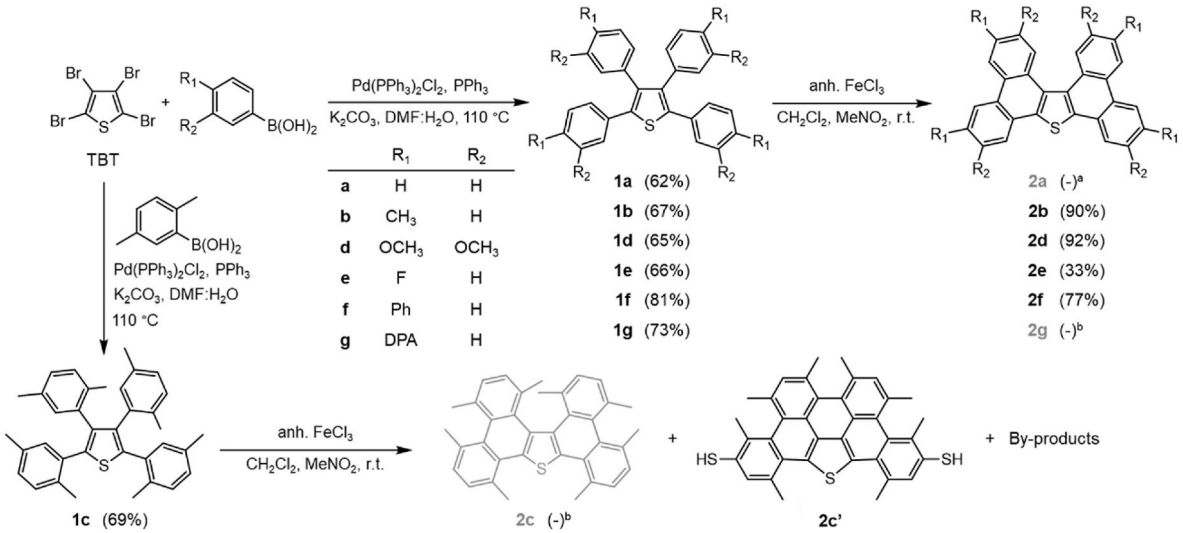

Scheme 1. Synthesis of tetrasubstituted compounds **1a–g** through a fourfold Suzuki-Miyaura cross-coupling reaction using tetrabromothiophene (TBT) and their subsequent cyclization towards **2a–g** through the Scholl reaction.
[a] The yield could not be estimated due to the complexity of the resultant mixture. [b] Not detected.

demonstrating excellent regioselectivity for the *para-para* cyclization with respect to the methoxy groups labeled as R_2. The incorporation of fluorine as an electron-withdrawing group in **1e** slowed the pace of the reaction to **2e**, affording a lower yield of 33 % after 72 h. Contrarily, the proposed strategy failed in yielding compounds **2a**, **2c** and **2g** due to the formation of alternative by-products. In fact, *ortho*- and *para*-positions are prone to undergoing undesired couplings, making them particularly vulnerable to these type of reactions [50]. Additionally, the cyclization to **2c** was further hampered by its highly constrained design, leading to a complex mixture of trace-level by-products from which compound **2c'** could be conveniently isolated and crystallized. Its structure, elucidated from the single crystal and depicted in Scheme 1, sheds light on the multiple side reactions that can occur when the main cyclization reaction is hindered by structural elements. The details of the single crystal structure can be found in the Supporting Information (Fig. S1, Table S1).

The synthesis of the unsubstituted compound **2a** was therefore projected via an alternative method proposed by Maddala et al. [39], which was slightly adapted and optimized from the original procedure (Scheme 2). In this strategy, 2-biphenylboronic acid was coupled to 2, 5-dibromothiophene (DBT), which replaced TBT as the starting material, in a 2-fold Suzuki-Miyaura reaction to form intermediate **3** in a yield of 86 %. Then, the Scholl reaction was carried out at a lower temperature of 0 °C for a more controlled arene-thiophene coupling in positions 3 and 4 of the thiophene, successfully affording compound **2a** in an overall yield of 77 % considering both steps. These modifications imply a 20 % increase from the original conditions [39].

In the case of **1g**, the Scholl reaction could theoretically lead to multiple arene-arene intra- and intermolecular couplings. This was corroborated with a complex mixture of by-products in which the target compound **2g** was not detected.

3.2. Thermal, electrochemical and semiconducting properties

The thermal stability of the cyclized compounds **2a,b,d–f**, evaluated by thermogravimetric analysis (TGA), revealed a significant increase in the decomposition temperature from 257 °C for the unsubstituted compound **2a** to approximately 400 °C for compounds **2b,d–f**. These results show that these compounds exhibit remarkably good thermal stability, essential for vacuum-deposition processes. Detailed thermal characterization data are available in the Supporting Information (Fig. S2).

The electrochemical behavior of the cyclized structures was analyzed in dichloromethane through cyclic voltammetries (CV). All derivatives underwent an oxidation process, so their ionization potentials (IP_{CV}) could be conveniently extracted from their first oxidation step (Table 1, Fig. S3). The analyzed **2**-based compounds displayed rather high ionization potentials close to 6 eV. As expected, the inclusion of stronger electron-donating groups (i.e. methyl, phenyl and methoxy groups in **2b**, **2f** and **2d**, respectively) derives into a destabilization of the HOMO energy level, thus decreasing their IP values up to 5.79 eV in the case of **2d**. Conversely, the addition of fluorine as an electro-withdrawing group in **2e** results in the opposite effect, with an exceptionally high IP value of 6.27 eV. Furthermore, their IP values in the solid state were also analyzed on vacuum-deposited thin-films using photoemission spectroscopy (IP_{PE}, Fig. S4). In this case, IP_{PE} showed rather lower values with respect to IP_{CV}, ranging from 5.96 eV for **2a** to 4.83 eV for **2d**. This discrepancy in the obtained IP_{CV} and IP_{PE} can be attributed to the distinct molecular interactions and arrangements present in solid layers compared to diluted solutions [51].

The characterization of their charge-transporting properties was carried out through the time of flight (TOF) technique utilizing vacuum-evaporated films of compounds **2a,b,d–f** sandwiched between Al electrodes and the ITO-coated glass substrate. The transient curves in the linear scale exhibited a dispersive pattern for all films. Therefore, the transient times were extracted from the inflection point of the photocurrent transient represented in the log-log scale (Figs. S5 and S6). The resulting hole mobilities (μ_h) ranged from 5.6×10^{-6} to 4.7×10^{-5} $cm^2 V^{-1} s^{-1}$ at a high electric field up to 6×10^5 V cm^{-1}. The best results

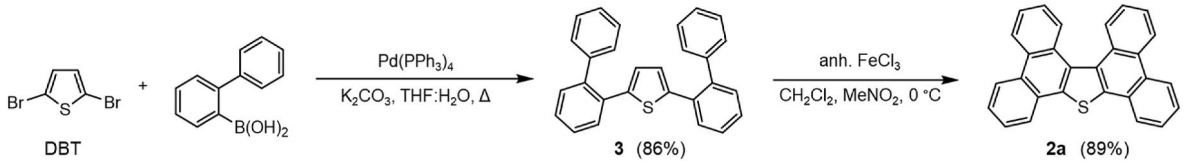

Scheme 2. Alternative synthetic pathway towards compound **2a** using 2,5-dibromothiophene (DBT) as the starting material.

Table 1
Optical energy gap, electrochemical and hole mobility data of compounds **2a,b, d–f**.

	E_{gap}^{opt} (eV)[a]	E_{onset}^{ox} (V)[b]	IP_{CV} (eV)[c]	EA (eV)[d]	IP_{PE} (eV)[e]	μ_h (cm^2 V^{-1} s^{-1})[f]	μ_0 (cm^2 V^{-1} s^{-1})[g]	α ($cm^{1/2}$ $V^{-1/2}$)[h]
2a	3.33	0.83	6.22	2.89	5.96	–	–	–
2b	3.24	0.58	5.97	2.73	5.21	5.6×10^{-6}	4.1×10^{-8}	6.6×10^{-3}
2d	3.14	0.40	5.79	2.65	4.83	3.9×10^{-5}	3.7×10^{-6}	2.8×10^{-3}
2e	3.27	0.88	6.27	3.00	5.55	–	–	–
2f	3.04	0.57	5.96	2.92	5.20	4.7×10^{-5}	4.6×10^{-7}	6.0×10^{-3}

[a] Optical band gap energy, estimated from the absorption spectrum.
[b] Onset oxidation potential vs. Fc^+/Fc estimated from CV in a 1 mM CH_2Cl_2 solution.
[c] Ionization potentials estimated as $IP_{CV} = E_{onset}^{ox} + 5.39$.
[d] Electronic affinity calculated as $EA = IP_{CV} - E_{gap}^{opt}$.
[e] Ionization potentials in the solid state extracted from the photoelectron emission spectra.
[f] Hole mobility at an electric field of ca. 6.0×10^5 V cm^{-1}.
[g] Zero-field mobility.
[h] Field dependence parameter. The thickness of the vacuum evaporated layers varied from 0.40 to 1.30 μm.

were obtained with derivatives **2d** and **2f**, which feature methoxy and phenyl groups, respectively. The presence of less electron-donating methyl groups in compound **2b** resulted in a 10-fold decrease, with a μ_h value of 5.6×10^{-6} cm^2 V^{-1} s^{-1}. Unfortunately, TOF measurements could not be performed on **2a** and **2e** due to the exceedingly crystalline nature of their films. Thus, the modulation of the diphenanthro[9,10-*b*:9′,10′-*d*]thiophene core to a more electron-rich configuration through the substitution pattern, especially if it also entails a π-extension of the system, is confirmed as a convenient approach towards new p-type semiconductors. Moreover, the lower IP values detected for **2d** and **2f** makes them suitable to be paired with the gold electrode work function (5.1 eV), paving the way to their potential application in final devices.

3.3. Optical properties

The optical properties of compounds **1a–g** and **2a,b,d–f** are summarized in Table 2 and Table S2. In dilute dichloromethane solutions, the open intermediates **1a–g** absorbed in the UV and emitted in the UV-deep blue region of the electromagnetic spectrum (Fig. 2a and b). In general, the addition of strong electron-donating groups induced a bathochromic shift to both the absorption and emission with respect to the unsubstituted compound **1a**, being more pronounced when aromatic substituents are attached (e.g. **1f** and **1g**) due to the extension of the conjugated system. The most significant change occurs with the addition of 4-(diphenylamino)phenyl moieties in **1g**, resulting in an even larger bathochromic shift of 72 and 57 nm with respect to **1a** in the absorption and emission spectra, respectively. This causes the absorption to shift

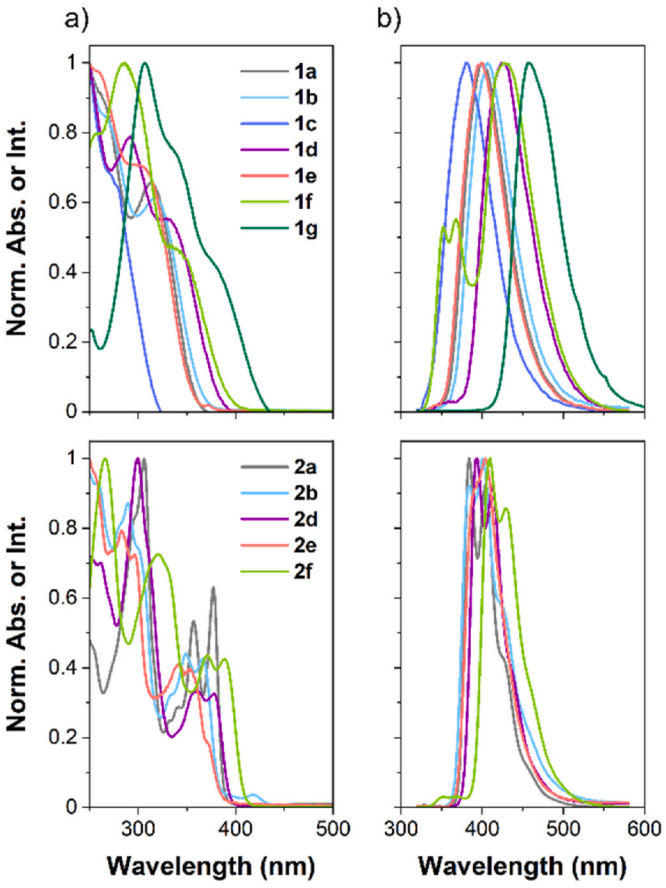

Fig. 2. Normalized absorbance (a) and PL (b) of compounds **1a–g** (above) and **2a,b,d–f** (below) in dichloromethane (10 μM).

towards the sky-blue region, while the emission shifts towards the blue-green zone. The results in the solid state showed similar profiles to those observed in solution, with a slight bathochromic shift in the absorption and a significant hypsochromic one in the emission (Fig. S7a and b). Most compounds exhibited PLQY values around 2.0 % as reported for similar species [52,53], with no significant impact from the side substituents except for **1f** and **1g,** which again diverged from the rest with markedly higher PLQYs of 9.9 % and 11.3 %, respectively. In contrast, the highly restricted structure of **1c** seemingly derives into a loss of π-conjugation between the thiophene nucleus and the 2,5-dimethyl phenyl scaffolds. Its optical properties are indeed closer to those of the isolated heterocycles [54] than to those of the unsubstituted analogue **1a**. All PLQY values in the solid state slightly drop with regard to their solution counterparts, corroborating that tetraphenylthiophene does not claim the notorious AIE of other propeller-shaped structures like 1,2,3,4-tetraphenyl-1,3-cyclopentadiene [52,55].

The Scholl reaction towards **2a,b,d–f** induces a slight red-shift to the

Table 2
Optical properties of the non-cyclized intermediates **1a–g** and their cyclized counterparts **2a,b,d–f** in dichloromethane solution and drop-casted films.

	Solution			Film			Solution			Film	
	$\lambda_{abs,onset}$ (nm)	$\lambda_{em,max}$ (nm)	PLQY[a] (%)	$\lambda_{em,max}$ (nm)	PLQY (%)		$\lambda_{abs,onset}$ (nm)	$\lambda_{em,max}$ (nm)	PLQY[a] (%)	$\lambda_{em,max}$ (nm)	PLQY (%)
1a	358	400	2.0	398	1.0	**2a**	387	394	3.2	449, 481	4.7
1b	363	406	2.4	397	1.0	**2b**	383	384, 400	6.1	497	7.6
1c	318	381	0.5	391	<0.1						
1d	382	424	3.2	409	1.0	**2d**	395	393, 412	8.0	436	1.1
1e	354	396	1.7	395	0.6	**2e**	379	403	4.0	427	2.4
1f	392	428	9.9	444	3.0	**2f**	408	409, 429	27.5	474	5.7
1g	430	457	11.3	433	2.7						

[a] Evaluated in a dilute solution of toluene.

absorption spectra with respect to their precursors, both in solution (Fig. 2a) and in the solid state (Fig. S7c), that is attributed to the expansion of the π-system. This tendency also relates to the emission spectra in the solid state (Fig. S7d), whereas a small hypsochromic shift occurs in solution (Fig. 2b), placing them in the sky-blue region for the former conditions and in the UV-blue for the latter ones. Moreover, the higher π-extension of compounds **2a,b,d–f** grants improved PLQYs, both in solution and in the solid state, with values for the unsubstituted core **2a** of 3.2 % and 4.7 %, respectively. This increase in the solid state is also detected in the case of the methylated **2b**. The inclusion of phenyl moieties in **2f** leads to the maximum PLQY in solution of 27.5 %, which drops to 5.7 % in the solid state resulting from aggregation-induced quenching.

Nevertheless, the main interest in the diphenanthro[9,10-*b*:9′,10′-*d*] thiophene core resides on its potential RTP. Under air-equilibrated conditions, oxygen quenches the T_1 efficiency by removing population from this state through non-radiative pathways. Hence, the emissive behavior of these compounds under air and vacuum conditions was compared in Zeonex-based films containing the fluorophore (1 % wt.), as compiled in Table 3 and Figure S9–S13a,b. Zeonex acts as an inert and rigid polymeric host matrix, which suppresses undesired vibrational relaxation processes that would otherwise promote the dissipation of the excited T_1 to the ground state.

All compounds exhibited a slight depletion in intensity of the prompt fluorescence under vacuum, while preserving the wavelength of the main fluorescence emission peak. Simultaneously, the broad band that appears at ca. 580–590 nm for all compounds hints yellow-orange RTP, suggesting the activation of phosphorescent emission in the absence of oxygen. The delayed (100 μs and 1 ms) PL spectra revealed that this band is also visible in all compounds, confirming its phosphorescent origin. Indeed, phosphorescence lifetimes (τ_{Phos}) showed values in the millisecond scale, ranging from 89 to 181 ms, in contrast to the fluorescence lifetimes (τ_{Fl}), placed in the nanoscale range for both air-equilibrated and vacuum conditions. Details on the lifetime measurements are shown in Figure S9–S13c,d and Table S3 of the Supplementary Information. Contrastingly, the PL spectra of the non-cyclized derivatives **1a–g** hardly changed when transitioning from air to vacuum conditions, evidencing the deficiency of triplet state radiative emission in these structures (Fig. S8). The PL spectra of the unsubstituted **1a** and its cyclized counterpart **2a** under air and vacuum conditions are depicted in Fig. 3a and b as representatives. The presence of RTP in the diphenanthro[9,10-*b*:9′,10′-*d*]thiophene core was further corroborated by investigating the temperature-dependence of the emission. The PL spectra of compound **2a** in a THF solution at 298 K and 77 K are shown in Fig. 3c. As observed, lowering the temperature from 298 K to 77 K prompts the appearance of a broad emission band peaking at 533 nm, indicating the T_1 to S_0 deexcitation characteristic of phosphorescence. This enhancement of the PL at low temperatures supports the identification of this phenomenon as RTP in contrast to TADF, in which the reverse intersystem crossing process (T_1 to S_1) would dominate. The singlet and triplet energy levels, as well as the corresponding ΔE_{ST} values, were extracted from Zeonex-doped films of compounds **2a,b,d–f**, and from THF solution spectrum of **2a** (Table S4). For compound **2a**, ΔE_{ST} is 0.96 eV in THF solution and 1.00 eV in Zeonex, values that are consistent with previously reported data for DBT. Upon functionalization, ΔE_{ST} further decreased to values as low as 0.86 eV for compounds **2d** and **2f**. In contrast, 2,5-diphenylthiophene, a structurally related compound to the open intermediates **1a–g**, has a significantly higher reported ΔE_{ST} (1.30 eV), which correlates with the absence of RTP in the open structures [35]. Temperature-dependent experiments on **1a–g** also failed in detecting phosphorescence, as shown in Fig. S14. Overall, these experiments highlights the importance of the Scholl reaction in the formation of the diphenanthro[9,10-*b*:9′,10′-*d*]thiophene core as a key step for facilitating ISC and unlocking RTP in these compounds.

Quantitatively, the PL intensity increases from air to vacuum conditions, expressed as the I_{vac}/I_{air} ratio, between 1.2 and 4.5, with **2a** and **2d** featuring the most notable improvement in the absence of air. The benchmark **2a** also exhibited the highest ratio between phosphorescence and fluorescence under vacuum (I_{Phos}/I_{FL}), with a value of 4.1. For the methylated (**1b**) and fluorinated (**1e**) derivatives, the I_{Phos}/I_{FL} ratios hovered around 1, implying certainly balanced contributions. However, extending conjugation through phenyl substituents in **2f** significantly reduced the I_{Phos}/I_{FL} ratio to 0.3, reflecting minimal RTP contribution. PLQY values of compounds **2a,b,d–f** within Zeonex in air are roughly similar to those in solution. Under vacuum, PLQY encompassing fluorescence and RTP goes from 9.6 (**2e**) to 24.5 % (**2f**), with RTP contributions up to 10 % for **2a** and **2d**.

Although the addition of side-groups to the parent structure negatively impacts RTP to varying extents, it offers a tunable and effective strategy to adjust the I_{Phos}/I_{FL} ratio and, consequently, the emitted color. Indeed, compounds **2a,b,d,e** exhibit a rather balanced contribution of deep-blue fluorescence and orange RTP that translates into white light emission, which is greatly sought-after for lighting applications. Indeed, single white light organic emitters are rarely reported in the literature [56–58] and offer greater stability while reducing the manufacture complexity when compared to multi-component white emitters [59]. This can be quantitatively interpreted using the *Commission Internationale de l'éclairage* (CIE) 1931 *x,y* chromaticity space, showing that the CIE coordinates for **2a,b,d,e** in vacuum are close to the Planckian locus (Fig. 3d). Specifically, CIE coordinates for **2b** and **2e** are (0.37, 0.32) and (0.42, 0.43), with correlated color temperatures (CCTs) of 4078 K and 3470 K, respectively, indicating neutral-white light emission. In contrast, the non-substituted compound **2a** and methoxy-substituted compound **2d** feature CIE coordinates of (0.47, 0.47) and (0.43, 0.39) respectively, with CCTs near 3000 K, characteristic of warm-white light emission. Thus, the incorporation of carefully

Table 3
Optical properties of Zeonex-based films containing compounds **2a,b,d–f** (1 % wt.).

	λ_{em} (nm)[a]	$\tau_{FL,air}$ (ns)[b]	$\tau_{FL,vac}$ (ns)[b]	τ_{Phos} (ms)[b]	I_{vac}/I_{air}[c]	I_{Phos}/I_{FL}[d]	Φ_{FL}, (%)[e]	Φ_{vac}, (%)[f]	Φ_{RTP} (%)[g]	$CIE_{,air}$[h]	$CIE_{,vac}$[h]	CCT (K)[i]
2a	393 (585)	0.70	0.70	154	4.5	4.1	2.7	12.2	9.8	(0.17, 0.04)	(0.47, 0.47)	3007
2b	401, 429 (590)	1.93	1.92	130	2.0	1.5	5.3	10.6	6.4	(0.17, 0.09)	(0.37, 0.32)	4078
2d	412 (585)	0.69	0.63	181	5.4	2.7	2.6	14.0	10.2	(0.21, 0.13)	(0.43, 0.39)	2931
2e	402 (579)	1.07	1.07	151	2.9	1.3	3.3	9.6	5.4	(0.22, 0.16)	(0.42, 0.43)	3470
2f	431 (584)	0.80	0.80	88.5	1.2	0.3	20.4	24.5	5.7	(0.16, 0.06)	(0.24, 0.12)	–

[a] Maximum emission wavelength in air (the values in parenthesis correspond to the maximum RTP wavelength that appears under vacuum).
[b] Lifetimes of fluorescence under aerated ($\tau_{FL,air}$) and vacuum ($\tau_{FL,vac}$) conditions and phosphorescence (τ_{Phos}) under vacuum.
[c] Ratio of overall PL intensity under aerated and vacuum conditions calculated as: $I_{vac}/I_{air} = Area_{vac}/Area_{air}$.
[d] Ratio of PL intensity from phosphorescence and fluorescence contributions under vacuum calculated as: $I_{Phos}/I_{FL} = Area_{Phos}/Area_{FL}$.
[e] PLQY values (Φ_{FL}) of fluorescence (FL) were measured in air using an integrating sphere.
[f] PLQY values under vacuum (Φ_{vac}) estimated as $\Phi_{vac} = (I_{vac}/I_{air})\Phi_{FL}$.
[g] PLQY values of RTP under vacuum (Φ_{RTP}) estimated as $\Phi_{RTP} = (I_{Phos}/(I_{Phos} + I_{FL,vac}))\Phi_{vac}$.
[h] CIE 1931 coordinates calculated from the corresponding PL spectra under aerated (h) and vacuum (i).
[i] Correlated color temperature (CCT) calculated from the corresponding CIE coordinates under vacuum conditions using the McCamy's approximation [45].

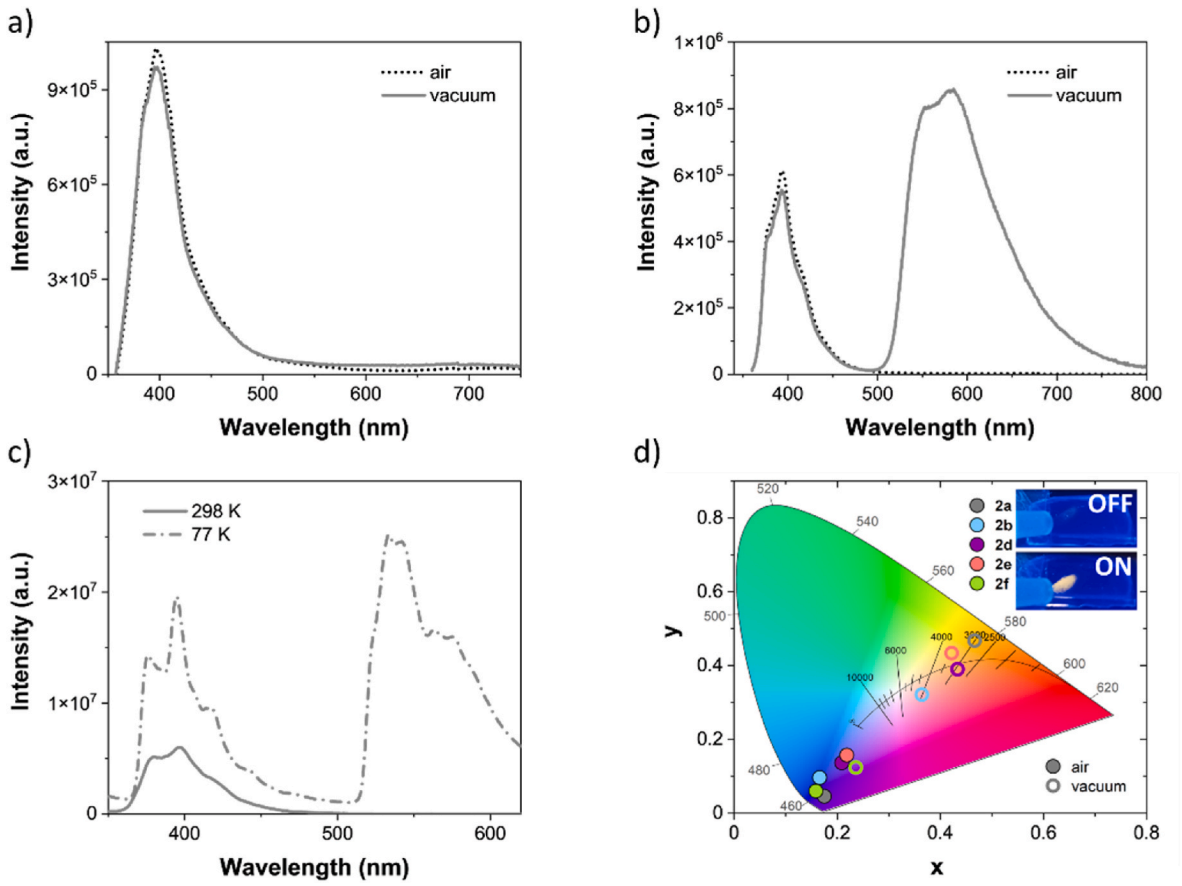

Fig. 3. a) PL spectra of a **1a** film in Zeonex (1 % wt.) under aerated (straight line) and vacuum conditions (dotted line). b) PL spectra of **2a** film in Zeonex (1 % wt.) under aerated (straight line) and vacuum conditions (dotted line). c) PL spectra of **2a** in THF solution at 298 K (straight line) and 77 K (dashed line). d) Correlated color coordinates represented in the CIE 1931 color space chromaticity diagram with the Planckian locus (the transversal lines indicate the color temperatures in K) and qualitative emission of a **2a**-doped Zeonex film with and without flush of argon.

chosen substituents permits to fine-tune the white hue within a wide scope of CCTs under vacuum via the modulation of the I_{Phos}/I_{FL} ratio. These results stress out the potential of diphenanthro[9,10-*b*:9′,10′-*d*] thiophene as a highly accessible, tunable and halogen-free core displaying RTP, offering significant potential for next-generation optoelectronic applications.

4. Conclusions

A family of diphenanthro[9,10-*b*:9′,10′-*d*]thiophene derivatives featuring diverse substituents was successfully synthetized through a straightforward two-step synthetic route. As revealed via photoemission spectroscopy, the exceedingly high ionization potential of the unsubstituted core **2a** in the solid state could be conveniently reduced from 5.96 eV to a scope of 4.83–5.26 eV with the inclusion of suitable substituents, closely approaching the gold work function (5.1 eV) for a potential OFET application. Indeed, their capability as hole-transporting materials was demonstrated by means of TOF measurements, with μ_h values up to 4.7×10^{-5} $cm^2\ V^{-1}\ s^{-1}$ at an electric field of 6×10^5 $V\ cm^{-1}$ for the phenyl-substituted system. Optical characterization in solution also revealed interesting deep-blue PL and PLQY values up to 27.5 % after functionalization. The emission in drop-casted films generally red-shifted to the sky blue-green region for all compounds, and slightly increased the PLQY values of derivatives **2a,b**, from 3.2 % to 4.7 % and 6.1 % to 7.6 % in solution and in films, respectively. Further investigation of their photophysical properties in Zeonex-based films unveiled prompt fluorescence coupled with millisecond-range orange RTP emission under vacuum, which was confirmed through temperature-dependent experiments. The balanced I_{Phos}/I_{FL} ratios for **2a,b,d,e** translated into an overall white-light emission, with values ranging from 1.3 to 4.1. Specifically, the CIE coordinates for **2b** and **2e** indicate neutral white-light emission, with CCT values in the range of 3500–4000 K. In contrast, **2a** and **2d** exhibit CIE coordinates that align with warm-white light. Therefore, the resulting white hue can be readily fine-tuned by carefully selecting the side groups in the diphenanthro[9,10-*b*:9′,10′-*d*]thiophene core. Conversely, analogous measurements for the open intermediates **1a–g** revealed the absence of RTP, highlighting the critical role of the rigidity conferred via the Scholl reaction in facilitating this luminescent behavior. These results emphasize the significant potential of the diphenanthro[9,10-*b*:9′,10′-*d*]thiophene nucleus as a highly-accessible halogen-free option towards single-component white-light emitting devices, paving the way for their application in next-generation optoelectronic devices.

CRediT authorship contribution statement

Clara Fabregat: Writing – original draft, Investigation, Data curation. **Roger Bujaldón:** Writing – original draft, Methodology, Investigation. **Jaume Garcia-Amorós:** Writing – review & editing. **Dmytro Volyniuk:** Validation, Supervision. **Melika Ghasemi:** Investigation, Data curation. **Juozas V. Grazulevicius:** Supervision, Funding acquisition. **Dolores Velasco:** Writing – review & editing, Funding acquisition, Conceptualization.

Associated content

The following files are available in the Supporting Information free of charge. Characteristics, ORTEP and interactions of the single crystal of **2c'** (Table S1, Fig. S1), thermal properties (Fig. S2), cyclic voltammetries (Fig. S3) and photoemission spectra (Fig. S4) of **2a,b,d-f**, TOF measurements of **2b,d,f** (Figs. S5 and S6), optical properties of solution and of films of **1a–g** and **2a,b,d–f** (Fig. S7, Table S2), and of Zeonex films of **1b–g** (Fig. S8) and of **2a,b,d-f** (Fig. S9–S13, Table S3), experimental singlet and triplet energies and ΔE_{ST} of compounds **2a,b,d–f** (Table S4), PL spectra of **1a–g** at 77 K in THF (Fig. S14), ^{1}H and ^{13}C NMR spectra of **2a,b,d–f**.

Declaration of competing interest

The authors declare that they have no known competing financial interests or personal relationships that could have appeared to influence the work reported in this paper.

Acknowledgments

Authors acknowledge the financial support by the Ministerio de Economía, Industria y Competitividad (grant numbers FUNMAT-PGC2018-095477-B-I00 and PID2023-151915NB-I00) and Horizon Europe, the European Union's framework programme for research and innovation (R&I) for 2021–2027, project HELIOS (grant agreement No 101155017). C.F and R.B are grateful for the predoctoral grant FI AGAUR from Generalitat de Catalunya. The authors want to also thank the CCiTUB for the use of their equipment, especially to Mercè Font of the X-Ray Diffraction Unit for the single-crystal elucidation.

Appendix A. Supplementary data

Supplementary data to this article can be found online at https://doi.org/10.1016/j.dyepig.2025.113053.

Data availability

Data will be made available on request.

References

[1] Fujiseki T, Fujimoto S, Campoy-Quiles M, Alonso MI, Murakami TN, Miyadera T, et al. Organic semiconductors. Springer Opt Sci 2018;214:427–69.
[2] Bronstein H, Nielsen CB, Schroeder BC, McCulloch I. The role of chemical design in the performance of organic semiconductors. Nat Rev Chem 2020;4:66–77.
[3] Hu P, He X, Jiang H. Greater than 10 $cm^2 V^{-1} s^{-1}$: a breakthrough of organic semiconductors for field-effect transistors. InfoMat 2021;3:613–30.
[4] Nikolka M, Nasrallah I, Rose B, Ravva MK, Broch K, Sadhanala A, et al. High operational and environmental stability of high-mobility conjugated polymer field-effect transistors through the use of molecular additives. Nat Mater 2017;16:356–62.
[5] Chen X, Wang Z, Qi J, Hu Y, Huang Y, Sun S, et al. Balancing the film strain of organic semiconductors for ultrastable organic transistors with a five-year lifetime. Nat Commun 2022;13:1480.
[6] Arias AC, MacKenzie JD, McCulloch I, Rivnay J, Salleo A. Materials and applications for large area electronics: solution-based approaches. Chem Rev 2010;110:3–24.
[7] Zhu H, Shin E, Liu A, Ji D, Xu Y, Noh Y. Printable semiconductors for backplane TFTs of flexible OLED displays. Adv Funct Mater 2020;30:1–36.
[8] Wallwork NR, Mamada M, Shukla A, McGregor SKM, Adachi C, Namdas EB, et al. High-performance solution-processed red hyperfluorescent OLEDs based on cibalackrot. J Mater Chem C Mater 2022;10:4767–74.
[9] Zeng X-Y, Tang Y-Q, Cai X-Y, Tang J-X, Li Y-Q. Solution-processed OLEDs for printing displays. Mater Chem Front 2023;7:1166–96.
[10] Allard S, Forster M, Souharce B, Thiem H, Scherf U. Organic semiconductors for solution-processable field-effect transistors (OFETs). Angew Chem Int Ed 2008;47:4070–98.
[11] Zhang C, Chen P, Hu W. Organic field-effect transistor-based gas sensors. Chem Soc Rev 2015;44:2087–107.
[12] Surya SG, Raval HN, Ahmad R, Sonar P, Salama KN, Rao VR. Organic field effect transistors (OFETs) in environmental sensing and health monitoring: a review. TrAC Trends Anal Chem 2019;111:27–36.
[13] Yuan X, Zhao Y, Xie D, Pan L, Liu X, Duan C, et al. Polythiophenes for organic solar cells with efficiency surpassing 17. Joule 2022;6:647–61.
[14] Li Y, Xu G, Cui C, Li Y. Flexible and semitransparent organic solar cells. Adv Energy Mater 2018;8:1–28.
[15] Zhi J, Zhou Q, Shi H, An Z, Huang W. Organic room temperature phosphorescence materials for biomedical applications. Chem Asian J 2020;15:947–57.
[16] He Z, Gao H, Zhang S, Zheng S, Wang Y, Zhao Z, et al. Achieving persistent, efficient, and robust room-temperature phosphorescence from pure organics for versatile applications. Adv Mater 2019;31:1–8.
[17] Han Y, You Y, Lee Y, Nam W. Double action: toward phosphorescence ratiometric sensing of chromium ion. Adv Mater 2012;24:2748–54.
[18] Wang X, Ma H, Gu M, Lin C, Gan N, Xie Z, et al. Multicolor ultralong organic phosphorescence through alkyl engineering for 4D coding applications. Chem Mater 2019;31:5584–91.
[19] Pander P, Swist A, Soloducho J, Dias FB. Room temperature phosphorescence lifetime and spectrum tuning of substituted thianthrenes. Dyes Pigments 2017;142:315–22.
[20] Lee D, Bolton O, Kim BC, Youk JH, Takayama S, Kim J. Room temperature phosphorescence of metal-free organic materials in amorphous polymer matrices. J Am Chem Soc 2013;135:6325–9.
[21] Lee DR, Park J, Lee JY. Metal and halogen-free purely organic room temperature phosphorescence material using heavy atom effect of phenoselenazine. Org Electron 2022;106:106534.
[22] Andruleviciene V, Leitonas K, Bernard RS, Woon KL, Volyniuk D, Sini G, et al. A multi-functional new acceptor for ultra-broad multiple emission, long-persistence thermally activated delayed fluorescence and room temperature phosphorescence. Adv Opt Mater 2024;12:1–11.
[23] Malpicci D, Forni A, Botta C, Giannini C, Lucenti E, Marinotto D, et al. Dual fluorescence and RTP features of carbazole-cyclic triimidazole derivatives: the fluorophores' connectivity does matter. Dyes Pigments 2023;215:111274.
[24] Pander P, Swist A, Motyka R, Soloducho J, Dias FB, Data P. Thermally activated delayed fluorescence with a narrow emission spectrum and organic room temperature phosphorescence by controlling spin–orbit coupling and phosphorescence lifetime of metal-free organic molecules. J Mater Chem C Mater 2018;6:5434–43.
[25] Park IS, Min H, Yasuda T. Ultrafast triplet–singlet exciton interconversion in narrowband blue organoboron emitters doped with heavy chalcogens. Angew Chem Int Ed 2022;61.
[26] Hua T, Zhan L, Li N, Huang Z, Cao X, Xiao Z, et al. Heavy-atom effect promotes multi-resonance thermally activated delayed fluorescence. Chem Eng J 2021;426:131169.
[27] Wang Z, Cheng X, Xie Y, Liu S, Dong M, Zhao J, et al. Recent advances in organic room-temperature phosphorescence of heteroatom (B/S/P)-Containing chromophores. CCS Chem 2023;5:292–309.
[28] Shudo H, Wiesener P, Kolodzeiski E, Mizukami K, Imoto D, Mönig H, et al. Thiophene-fused aromatic belts. Nat Commun 2025;16:1074.
[29] Zeng C, Deng W, Zhao K, Redshaw C, Donnio B. Phenanthrothiophene-triazine star-shaped discotic liquid crystals: Synthesis, self-assembly, and stimuli-responsive fluorescence properties. Chem Eur J 2024;30.
[30] Zhang D, Zhao C, Zheng X, Wu L, Xu J, Zhou L, et al. A study on the luminescence properties of high-performance benzothieno[3,2-*b*][1]benzothiophene based organic semiconductors. Dyes Pigments 2023;216:111359.
[31] Reineke S, Baldo MA. Room temperature triplet state spectroscopy of organic semiconductors. Sci Rep 2014;4:3797.
[32] El-Sayed MA. Triplet state. Its radiative and nonradiative properties. Acc Chem Res 1968;1:8–16.
[33] Baryshnikov G, Minaev B, Ågren H. Theory and calculation of the phosphorescence phenomenon. Chem Rev 2017;117:6500–37.
[34] Fang X, Yan D. White-light emission and tunable room temperature phosphorescence of dibenzothiophene. Sci China Chem 2018;61:397–401.
[35] Wasserberg D, Marsal P, Meskers SCJ, Janssen RAJ, Beljonne D. Phosphorescence and triplet state energies of oligothiophenes. J Phys Chem B 2005;109:4410–5.
[36] Zander M. Zur Photolumineszenz von Benzologen des Thiophens. Z Naturforsch 1985;40:497–502.
[37] Cossu S, De Lucchi O, Fabbri D, Valle G, Painter GF, Smith RAJ. Synthesis of structurally modified atropisomeric biaryl dithiols. Observations on the newman-kwart rearrangement. Tetrahedron 1997;53:6073–84.
[38] Jang JH, Ahn S, Park SE, Kim S, Byon HR, Joo JM. Synthesis of redox-active phenanthrene-fused heteroarenes by palladium-catalyzed C–H annulation. Org Lett 2020;22:1280–5.
[39] Maddala S, Panua A, Venkatakrishnan P. Steering scholl oxidative heterocoupling by tuning topology and electronics for building thiananographenes and their functional N−/C−Congeners. Chem Eur J 2021;27:16013–20.
[40] Venkateswarlu S, Lin Y-D, Lee K-M, Liau K-L, Tao Y-T. Thiophene-fused butterfly-shaped polycyclic arenes with a Diphenanthro[9,10- b :9′,10′- d]thiophene core for highly efficient and stable perovskite solar cells. ACS Appl Mater Interfaces 2020;12:50495–504.
[41] Venkateswarlu S, Prakoso SP, Kumar S, Tao Y. Accessing π-expanded heterocyclics beyond dibenzothiophene: syntheses and properties of phenanthrothiophenes. J Chin Chem 2020;67:437–45.
[42] Venkateswarlu S, Prakoso SP, Kumar S, Kuo M-Y, Tao Y-T. Benzophenanthrothiophenes: syntheses, crystal structures, and properties. J Org Chem 2019;84:10990–8.
[43] Zhao K, Du J, Wang H, Zhao K, Hu P, Wang B, et al. Board-like fused-thiophene liquid crystals and their benzene analogs: facile synthesis, self-assembly, p-type semiconductivity, and photoluminescence. Chem Asian J 2019;14:462–70.

[44] Cardona CM, Li W, Kaifer AE, Stockdale D, Bazan GC. Electrochemical considerations for determining absolute frontier orbital energy levels of conjugated polymers for solar cell applications. Adv Mater 2011;23:2367–71.
[45] McCamy CS. Correlated color temperature as an explicit function of chromaticity coordinates. Color Res Appl 1992;17:142–4.
[46] He F, Tian LL, Tian XY, Xu H, Wang YH, Xie WJ, et al. Diphenylamine-substituted cruciform oligo(phenylene vinylene): enhanced one- and two-photon excited fluorescence in the solid state. Adv Funct Mater 2007;17:1551–7.
[47] Krucaite G, Blazevicius D, Tavgeniene D, Grigalevicius S, Lin C-H, Shao C-M, et al. Tetramer of triphenylamine and similar derivatives with bromine atoms as hole injecting/transporting materials for efficient red phosphorescent OLEDs. Opt Mater 2020;108:110225.
[48] Erdoğan M, Horoz S. Synthesis and characterization of a triphenylamine-dibenzosuberenone-based conjugated organic material and an investigation of its photovoltaic properties. J Chem Res 2021;45:207–12.
[49] Kumar S, Tao Y-T. Synthesis of polyarylated carbazoles: discovery toward soluble Phenanthro- and Tetraceno-Fused carbazole derivatives. J Org Chem 2015;80:5066–76.
[50] King BT, Kroulík J, Robertson CR, Rempala P, Hilton CL, Korinek JD, et al. Controlling the scholl reaction. J Org Chem 2007;72:2279–88.
[51] Wang C, Ouyang L, Xu X, Braun S, Liu X, Fahlman M. Relationship of ionization potential and oxidation potential of organic semiconductor films used in photovoltaics. Sol RRL 2018;2:2–7.
[52] Nie H, Hu K, Cai Y, Peng Q, Zhao Z, Hu R, et al. Tetraphenylfuran: aggregation-induced emission or aggregation-caused quenching? Mater Chem Front 2017;1:1125–9.
[53] Xing Y, Xu X, Wang F, Lu P. Optical properties of a series of tetraarylthiophenes. Opt Mater 2006;29:407–9.
[54] Piotrowski P, Zarębska K, Skompska M, Kaim A. Electrodeposition and properties of donor-acceptor double-cable polythiophene with high content of pendant fulleropyrrolidine moieties. Electrochim Acta 2014;148:145–52.
[55] Stojanović L, Crespo-Otero R. Aggregation-induced emission in the tetraphenylthiophene crystal: the role of triplet states. J Phys Chem C 2020;124:17752–61.
[56] He Z, Zhao W, Lam JWY, Peng Q, Ma H, Liang G, et al. White light emission from a single organic molecule with dual phosphorescence at room temperature. Nat Commun 2017;8:416.
[57] Chen Z, Ho C, Wang L, Wong W. Single-molecular white-light emitters and their potential WOLED applications. Adv Mater 2020;32:1–45.
[58] Khan F, Volyniuk L, Ghasemi M, Volyniuk D, Grazulevicius JV, Misra R. Efficient monomolecular white emission of phenothiazine boronic ester derivatives with room temperature phosphorescence. J Mater Chem C Mater 2022;10:10347–55.
[59] Schwartz G, Pfeiffer M, Reineke S, Walzer K, Leo K. Harvesting triplet excitons from fluorescent blue emitters in white organic light-emitting diodes. Adv Mater 2007;19:3672–6.